Article

Discovery Medicine 2025; 37(199): 1493–1509
https://doi.org/10.24976/Discov.Med.202537199.130

Identification of Immune Evasion-Associated Genes in the Tumor Microenvironment of Hepatocellular Carcinoma and Development of a Prognostic Risk Model

ZhaoWen Bi[1], DeXue Fan[2], XinXing Wang[2], XiZhen Li[2], ZhenHai Zhang[3,4,5,*]

[1]Department of Hepatobiliary Surgery, Medical Integration and Practice Center, Shandong University, 250100 Jinan, Shandong, China
[2]Department of Hepatobiliary Surgery, Shandong Provincial Hospital Affiliated to Shandong First Medical University, 250014 Jinan, Shandong, China
[3]Shandong University, 250100 Jinan, Shandong, China
[4]Shandong First Medical University, 250117 Jinan, Shandong, China
[5]Department of Hepatobiliary Surgery, Dongying People's Hospital, 257091 Dongying, Shandong, China
*Correspondence: ZhenHaiZ2517@163.com (ZhenHai Zhang)
Published: 20 August 2025

Background: Hepatocellular carcinoma (HCC) is a major contributor to cancer-related mortality worldwide, with its progression significantly influenced by immune evasion mechanisms. This research aimed to identify key genes associated with immune evasion and assess their clinical significance in HCC.

Methods: Gene expression data from 342 HCC patients were obtained from The Cancer Genome Atlas (TCGA) repository. The Estimation of Stromal and Immune cells in Malignant Tumor tissues using Expression data (ESTIMATE) algorithm was employed to calculate immune and stromal scores. Differential gene expression analysis was conducted between high and low immune score groups, as well as between high and low stromal score groups. The resulting differentially expressed genes (DEGs) underwent functional enrichment analysis. A prognostic risk score model for HCC was constructed utilizing Least Absolute Shrinkage and Selection Operator (LASSO)-Cox, univariate, and multivariate Cox regression analyses. The prognostic performance of the model was evaluated through Kaplan-Meier survival analysis and receiver operating characteristic (ROC) curve analysis. Tumor and adjacent normal tissues from HCC patients were collected, and immune cell infiltration was quantified utilizing the Tumor Immune Estimation Resource (TIMER) database. Immunohistochemistry was performed to validate the expression of immune evasion-related proteins in clinical specimens.

Results: A total of 999 DEGs were identified from the immune and stromal score-based groups. These genes were predominantly enriched in immune-related pathways, including cytokine-cytokine receptor interactions, chemokine signaling, Wnt signaling, and the Hippo signaling pathway. Using univariate and multivariate Cox regression analysis, a prognostic model comprising six genes (Myocardin (*MYOCD*), Matrix Metallopeptidase 7 (*MMP7*), Matrix Metallopeptidase 16 (*MMP16*), PR/SET Domain 9 (*PRDM9*), Caudal Type Homeobox 2 (*CDX2*), and T Cell Receptor Beta Variable 10-3 (*TRBV10-3*)) was developed and demonstrated a significant association with overall survival (OS) in HCC patients ($p < 0.05$). The model yielded a concordance index (C-index) of 0.764, indicating robust prognostic performance. *MYOCD* was associated with a protective effect, showing an inverse correlation with the risk score ($p < 0.001$). Conversely, *MMP7*, *PRDM9*, *CDX2*, and *MMP16* were risk-associated, with their expression levels positively correlating with the risk score ($p < 0.001$), whereas *TRBV10-3* showed no significant difference between high- and low-risk groups ($p > 0.05$). Immunohistochemical validation confirmed the downregulation of MYOCD and upregulation of MMP7, MMP16, PRDM9, and CDX2 in HCC tissues ($p < 0.001$). Analysis of immune cell infiltration revealed a significant negative correlation between *MYOCD* expression and both stromal and ESTIMATE scores ($p < 0.001$), while *MMP7* and *MMP16* exhibited significant positive correlations with stromal, immune, and ESTIMATE scores ($p < 0.001$). *PRDM9* and *CDX2* also showed significant positive correlations with stromal scores ($p < 0.05$).

Conclusion: This study presents the first comprehensive identification of immune evasion-related genes (IERGs) within the tumor microenvironment (TME) of HCC and introduces a novel prognostic model based on immune evasion with strong clinical applicability. These findings offer valuable insights into the immunobiology of HCC and highlight potential therapeutic targets for precision immunotherapy.

Keywords: hepatocellular carcinoma; immune evasion; survival analysis; prognostic

Introduction

Recent data from the World Health Organization (WHO) indicate that liver cancer accounted for approximately 900,000 new diagnoses globally in 2020, ranking it as the seventh most prevalent malignancy and the third leading cause of cancer-related deaths. Hepatocellular carcinoma (HCC) constitutes about 75% of primary liver cancers and exhibits the highest mortality rates in Asia and Africa [1]. Due to the anatomical characteristics and physiological complexity of the liver, early diagnosis of HCC is challenging, and detection often occurs only at advanced stages. Delayed diagnosis, coupled with the malignant biological behavior of the tumor, contributes to the poor long-term survival outcomes associated with HCC [2]. Although recent advancements in hepatic cancer therapeutics, including surgical resection, liver transplantation, local ablation techniques, and targeted molecular interventions, have shown promise [3–5], recurrence and metastasis continue to pose significant challenges in treatment. Consequently, there remains a pressing need for effective strategies to evaluate prognosis and improve clinical outcomes.

Emerging evidence indicates that immune evasion mechanisms are implicated in the onset, progression, and therapeutic resistance of HCC. Immune evasion refers to the tumor's capacity to suppress the host immune system's recognition and clearance through various mechanisms, thereby facilitating tumor growth and metastasis. In HCC, the tumor microenvironment (TME) is the primary site of immune evasion, where tumor cells modulate immune responses by influencing immune cell infiltration, altering cytokine milieu, and upregulating immune checkpoint proteins such as Programmed Death-Ligand 1 (PD-L1) and Cytotoxic T-Lymphocyte-Associated Protein 4 (CTLA-4) [6,7]. Therefore, identifying molecular biomarkers associated with immune evasion and an in-depth understanding of their roles in the immune escape mechanisms of HCC are essential for early diagnosis, prognostic assessment, and the development of novel therapeutic strategies.

Despite the significant success of immune checkpoint inhibitors (ICIs) in other malignancies, such as non-small cell lung cancer [8], melanoma [9], and renal cell carcinoma [10], their efficacy in HCC remains limited [11]. A study demonstrated that the combination of atezolizumab (a PD-L1 inhibitor) and bevacizumab (an anti-Vascular Endothelial Growth Factor (VEGF) monoclonal antibody) significantly improves survival outcomes in advanced HCC patients, enhancing overall survival (OS) and progression-free survival (PFS) compared to sorafenib [12]. However, even optimized immune-based combination therapies achieve an objective response rate (ORR) of less than 30%, with only a fraction of patients experiencing long-term clinical benefits. This variability in efficacy is likely attributable to the distinct immune heterogeneity and complex immune escape mechanisms characteristic of HCC. Previous studies have revealed that several immunosuppressive factors such as tumor-associated macrophages, myeloid-derived suppressor cells, regulatory T cells (Tregs), transforming growth factor-beta (TGF-β), and interleukin-10 (IL-10) play crucial roles in the immune escape of HCC [13–15]. However, while considerable progress has been made in elucidating the fundamental mechanisms of immune escape, the clinical prognostic value of immune escape-related genes remains underexplored, and their integration into clinical stratification and precision therapy in HCC is still limited.

Currently, clinical prognostic evaluation of HCC primarily relies on pathological features such as tumor size, vascular invasion, and alpha-fetoprotein (AFP) levels. However, these models typically overlook immune escape mechanisms, limiting their utility in guiding immunotherapeutic decision-making [16]. Given that immune escape mechanisms strongly influence the development and progression of HCC, prognostic models incorporating immune escape-related genes may offer superior predictive value compared to conventional clinicopathological models. Such models can enable more precise identification of high-risk patients and inform the optimization of immunotherapeutic strategies. However, systematically identifying key immune escape genes in HCC and integrating them into clinically applicable prognostic models remains a significant scientific challenge. The objective of this study was to comprehensively characterize immune evasion-related genes in HCC, and, subsequently, to develop a novel predictive model based on these identified genes. The study integrated genomic datasets, bioinformatic analyses, and validation using clinical samples to investigate the molecular features of immune escape in HCC and reveal its potential clinical value. This model will enhance prognostic accuracy in HCC patients, facilitate the identification of individuals likely to benefit from immunotherapy and provide novel insights for personalized treatment approaches.

Methods

Data Retrieval and Expression Profile Assessment

The gene expression profile data used in this study were obtained from TCGA database (https://cancergenome.nih.gov/). To facilitate gene annotation, the mapping between gene symbols and Ensembl gene IDs (ENSG_IDs) was established using reference annotation files from the GENCODE database (https://www.gencodegenes.org/human/). Gene annotation files for versions v22 and v33 (General Feature Format version 3 (GFF3) format) were downloaded from the following sources: version v22 file (http://ftp.ebi.ac.uk/pub/databases/gencode/Gencode_human/release_22/gencode.v22.annotation.gff3.gz) and version v33 file (http://ftp.ebi.ac.uk/pub/databases/gencode/Gencode_human/release_33/gencode.v33.annotation.gff3.gz). From

these GFF3 files, the mapping relationship between gene symbols (GeneSymbol) and Ensembl gene IDs (ENSG_ID) was extracted and processed accordingly. In instances of multiple mappings, the median value was selected to ensure consistency and reliability of the data. The resulting gene expression matrix was used for subsequent analyses. During the imputation, an appropriate number of nearest neighbors (K) was chosen to complete the missing values, preserving data integrity and the robustness of subsequent analyses. Log_2 transformation [$\log_2(x + 1)$] was applied to normalize the data. Samples with missing clinical data were excluded, resulting in a final cohort of 342 HCC cases.

Identification of DEGs Based on Immune and Stromal Infiltration

The "estimate" R package was used to compute immune, stromal, and combined ESTIMATE scores. Based on the median values of these scores, patients were categorized into high- and low-score groups [17,18]. Differentially expressed genes (DEGs) between these groups were identified employing the Limma package (version 3.44.3), with DEGs defined by $|\log_2$ Fold Change (FC)$| > 1$ and a p-value < 0.05. For subsequent analyses, DEGs common to immune and stromal score groups were retained for further investigation.

Functional Enrichment Analysis

Gene Ontology (GO) annotations for human genes were retrieved using the org.Hs.eg.db package (version 3.1.0), while Kyoto Encyclopedia of Genes and Genomes (KEGG) pathway annotations were accessed through the KEGG REST API (https://www.kegg.jp/kegg/rest/keggapi.html). These annotations served as background references for gene mapping and enrichment analysis, which was conducted using the clusterProfiler R package (version 3.14.3). Gene sets containing fewer than 5 or more than 5000 genes were excluded for GO and KEGG enrichment analyses. Significance thresholds were set at a p-value < 0.05 and false discovery rate (FDR) <0.25.

Core Gene Selection and Prognostic Analysis

The Least Absolute Shrinkage and Selection Operator (LASSO) Cox regression method was employed using the glmnet R package to integrate survival time, survival outcome, and gene expression profiles. Tenfold cross-validation was conducted to identify the optimal model. To further assess the prognostic value of selected key genes, Cox regression analyses were performed using survival time, survival status, and corresponding gene expression data from the 342-sample cohort in the survival R package. The log-rank, Wald, and score tests were used to evaluate overall prognostic significance. Harrell's C-index was calculated to assess the model's capacity to discriminate between patients at different risk levels. A C-index approaching 1 indicates excellent discriminatory ability between high- and low-risk individuals. To further refine the optimal cutoff for the risk score, the Youden index method was employed to balance sensitivity and specificity, thereby enhancing the predictive performance of the model. The optimal risk score cutoff was determined using the maxstat R package (version 0.7-25). Patients were then stratified into high- and low-risk groups according to this cutoff value. Survival differences between the groups were assessed using the survfit function. The predictive performance of the risk model was evaluated by calculating the area under the receiver operating characteristic (ROC) curve (AUC) at 1, 3, and 5 years using the pROC R package (version 1.17.0.1).

Construction and Assessment of the Prognostic Model

A predictive model was developed using Cox regression within the rms package, incorporating survival time, survival status, and relevant covariates. A nomogram was constructed to represent the model and facilitate visualization. Calibration plots and ROC curves were used to evaluate the model's predictive performance and consistency.

Sample Collection and Clinicopathological Data Acquisition

The HCC tissue microarrays and normal liver tissue microarrays used in this study were purchased from Shanghai Outdo Biotech Co., Ltd., a commercial supplier of tissue microarrays. All tissue samples were pathologically confirmed and accompanied by comprehensive clinicopathological information, including patient age, gender, Tumor-Node-Metastasis (TNM) stage, tumor size, serum AFP levels, and liver function parameters. The supplier provided a formal statement regarding the legality, ethical compliance, and anonymization of the samples, in accordance with the principles outlined in the Declaration of Helsinki. As the samples used in this study were obtained from commercial tissue microarrays, and the research did not involve direct patient interaction or access to identifiable personal information, patient consent or institutional ethical approval was not required.

This study included 20 HCC tissue microarray samples and 24 normal liver tissue microarray samples. The normal liver tissues were sourced from either non-cancerous liver cases or from histologically confirmed non-tumorous regions located at least 5 cm from the tumor margin. All diagnoses were independently verified by certified pathologists. All data were used exclusively for this basic research and were kept strictly confidential, with no personally identifiable information being involved. Sample size calculation was based on prior literature and preliminary data. Using G*Power software (version 3.1, Heinrich Heine University Düsseldorf, Düsseldorf, Germany), a significance level (α) of 0.05, power ($1-\beta$) of 0.80, and an

expected effect size (Cohen's d) of 0.8, the minimum required sample size was estimated to be 16 per group. The actual sample size in this study exceeded this requirement, ensuring sufficient statistical power.

Immunohistochemical Analysis of Gene Expression

The tissue microarrays purchased for this study were snap-frozen, paraffin-embedded, and sectioned into 4 µm slices. Following deparaffinization and rehydration, antigen retrieval was performed using citrate buffer and microwave heating. Endogenous peroxidase activity was blocked using hydrogen peroxide, and non-specific binding was inhibited with bovine serum albumin (BSA). The primary antibodies used were Myocardin (MYOCD) (Proteintech, 12457-1-AP, 1:200, Wuhan, China), Matrix Metallopeptidase 7 (MMP7) (Abcam, ab207299, 1:100, Shanghai, China), Matrix Metallopeptidase 16 (MMP16) (Abcam, ab73877, 1:150, Shanghai, China), PR/SET Domain 9 (PRDM9) (Invitrogen, PA5-41161, 1:100, Waltham, MA, USA), and Caudal Type Homeobox 2 (CDX2) (Abcam, ab76541, 1:200, Shanghai, China). Tissue sections were incubated with these antibodies overnight at 4 °C. The next day, sections were incubated with HRP-conjugated secondary antibody (goat anti-rabbit IgG, ZB-2301, 1:500, ZSGB-BIO, Beijing, China) for 1 hour at room temperature. Staining was developed using DAB chromogenic solution (ZLI-9019, ZSGB-BIO, Beijing, China) for 3–5 minutes in the dark, followed by hematoxylin counterstaining for 30 seconds. Finally, slides were mounted using a transparent mounting medium and examined under an Olympus BX51 optical microscope (BX51, Olympus Corporation, Tokyo, Japan).

Assessment of the Relationship Between Gene Expression and Immune Cell Infiltration

Immune cell infiltration in HCC was assessed using the TIMER database (https://cistrome.shinyapps.io/timer/), integrated with transcriptomic data from tumor tissues of postoperative HCC patients. The abundance of various immune cell types, including T cells, B cells, dendritic cells, and macrophages, was quantified. Immune cell infiltration data were correlated with clinical characteristics to evaluate the impact of immune cell infiltration on patient prognosis. Spearman's correlation analysis was performed to evaluate the association between immune cell infiltration levels (or immune infiltration scores) and expression levels of target genes. Additionally, Kaplan-Meier survival analysis was conducted to investigate the association between immune cell infiltration and patient survival outcomes.

Statistical Analysis

R software (version 3.6.2, https://www.r-project.org, R Foundation for Statistical Computing, Vienna, Austria) was utilized for Cox regression, Kaplan-Meier (K-M) survival analysis, and LASSO regression. Data normality was assessed using SPSS 22.0 (SPSS Inc., Chicago, IL, USA). The Kolmogorov-Smirnov test was used to assess the distribution of continuous variables. For normally distributed variables, independent-sample *t*-tests were used to compare means between groups, with results expressed as mean ± standard deviation (mean ± SD), and *t* and *p*-values were recorded. Categorical variables were expressed as frequency and percentage [n (%)], and group comparisons were conducted using the chi-square, corrected chi-square, Fisher's exact test, or Fisher-Irwin test, with corresponding chi-square and *p*-values recorded. Statistical significance was set at $p < 0.05$.

Results

Differentially Expressed Genes Based on ESTIMATE Scores

According to the inclusion criteria, a total of 342 HCC patients were selected from the TCGA dataset. Using TCGA gene expression profiles, the ESTIMATE algorithm was employed to calculate stromal, immune, and combined scores. Gene expression variations were then examined among high and low stromal and immune score groups. We observed elevated expression of 979 genes and reduced expression of 145 genes in the stromal score group. Similarly, the immune score group exhibited 1412 genes with heightened expression and 283 genes with reduced expression (Fig. 1A). Venn diagram analysis identified 999 overlapping genes between the 1124 stromal DEGs and 1695 immune DEGs (Fig. 1B). These overlapping genes were designated as DEGs for downstream analyses.

Functional Enrichment Analysis of Differentially Expressed Genes

To explore the potential roles of the DEGs in immune escape within the HCC TME, GO functional annotation and KEGG pathway enrichment analyses were conducted. GO analysis revealed that the DEGs were primarily associated with immune-related biological processes, including adaptive immune response, complement activation, and regulation of immune response. In the cellular component (CC) category, the DEGs were primarily localized to the cell membrane, extracellular space, plasma membrane part, and extracellular matrix. For molecular function (MF), the DEGs were associated with antigen binding, receptor modulating activity, receptor-ligand interaction, signal receptor binding, and ion channel activity (Fig. 1C). KEGG pathway enrichment analysis demonstrated that the DEGs participated in immune responses, neuroactivity, and cancer-related pathways, including viral protein interaction with cytokine and cytokine receptor, cytokine-cytokine receptor interaction, chemokine signaling, Wnt signaling, and Hippo signaling pathway (Fig. 1D). These findings suggest that immune evasion may be mediated through these signaling pathways in the liver cancer microenvironment.

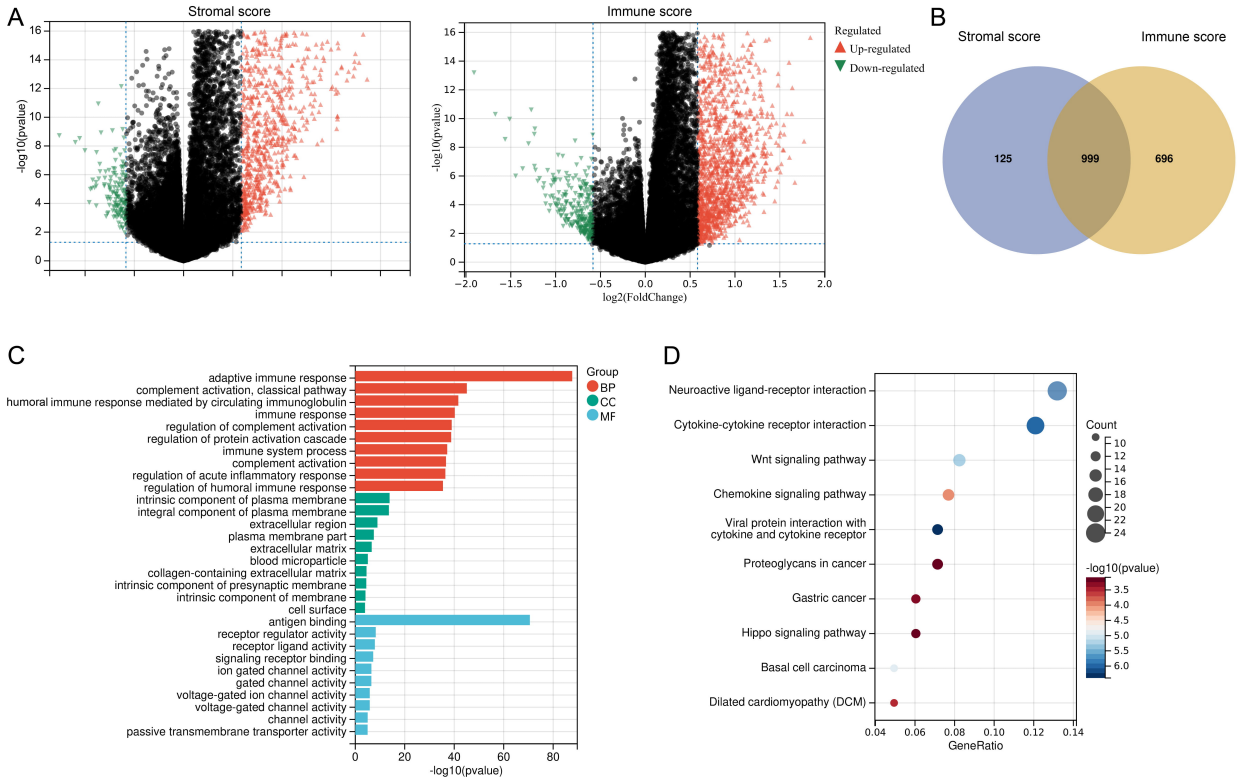

Fig. 1. Differential gene expression analysis based on stromal and immune scores. (A) Volcano plots illustrating differentially expressed genes (DEGs) among high and low stromal score groups (left) and high and low immune score groups (right). Upregulated genes are shown in red, while down-regulated genes are shown in green. (B) Venn diagram showing the intersection of DEGs from stromal and immune score comparisons, identifying 999 common DEGs. (C) Gene Ontology (GO) annotation analysis of the 999 shared DEGs, highlighting biological processes, cellular components, and molecular functions. (D) Kyoto Encyclopedia of Genes and Genomes (KEGG) pathway enrichment analysis of the shared DEGs (n = 999), indicating significantly enriched biological pathways. BP, biological process; CC, cellular component; MF, molecular function.

Core Gene Selection and Prognostic Model Construction

Using LASSO-Cox, along with univariate and multivariate Cox regression analyses, we developed a risk assessment model to predict prognosis in HCC patients by integrating gene expression profiles and survival data (time and status) from 342 individuals with HCC. Ten-fold cross-validation identified an optimal lambda value of 0.08, resulting in the selection of 15 genes to construct the risk score model (Fig. 2A). These genes included *MYOCD*, Pyroglutamylated RFamide Peptide Receptor (*QRFPR*), *MMP16*, C-Type Lectin Domain Family 1 Member B (*CLEC1B*), Lipocalin 6 (*LCN6*), *MMP7*, T Cell Receptor Beta Variable 10-3 (*TRBV10-3*), Uncharacterized Long Non-Coding RNA AC080038.4 (*AC080038.4*), *PRDM9*, Uncharacterized Long Non-Coding RNA AC022905.1 (*AC022905.1*), Shisa Family Member 9 (*SHISA9*), APCDD1L Divergent Transcript (Long Non-Coding RNA) (*APCDD1L-DT*), *CDX2*, Proteasome 26S Subunit, ATPase 1 Pseudogene 10 (*PSMC1P10*), and V-Set and Transmembrane Domain Containing 1 (*VSTM1*). Univariate and multivariate Cox regression analyses were performed using the survival package in R to evaluate the model's predictive performance (Fig. 2B,C). Genes with a p-value < 0.01 were selected for inclusion in the final model. Six genes (*MYOCD*, *TRBV10-3*, *MMP7*, *PRDM9*, *CDX2*, and *MMP16*) were identified, and their prognostic value was evaluated. The analysis shows a significant association between these genes and OS in HCC patients (log-rank test = 1.76×10^{-14}, score test = 6.57×10^{-17}, Wald test = 1.90×10^{-16}). The C-index was 0.764, suggesting that the model had robust prognostic predictive power.

Evaluation of the Risk Prediction Model and Survival Analysis

Kaplan-Meier survival analysis and ROC curve analysis were subsequently conducted to confirm the clinical predictive relevance of the risk score model. The Maxstat method determined the optimal risk score threshold of 0.54 (i.e., a risk score >0.54 was defined as the high-risk group and ≤ 0.54 as the low-risk group). This cutoff was further refined using the Youden index to optimize sensitivity and specificity, thereby enhancing the predictive accuracy of the model. Kaplan-Meier survival curves revealed a signif-

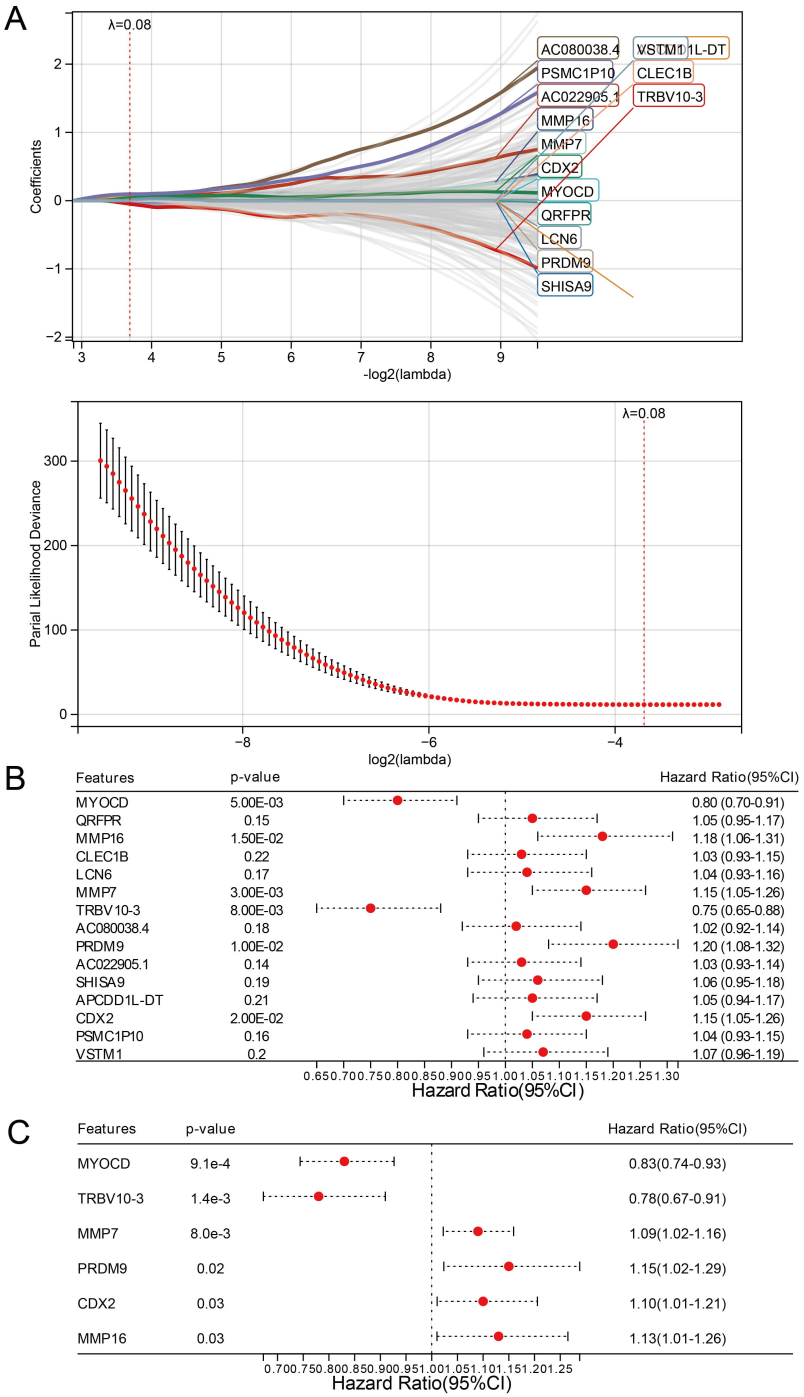

Fig. 2. Construction of a prognostic risk model for hepatocellular carcinoma (HCC) using Least Absolute Shrinkage and Selection Operator (LASSO)-Cox regression. (A) Selection of prognostic genes through LASSO-Cox regression analysis. The optimal lambda value ($\lambda = 0.08$) was determined through ten-fold cross-validation. Genes with non-zero coefficients were retained for model construction. (B) Univariate Cox proportional hazards regression analysis of candidate prognostic genes. (C) Multivariate Cox proportional hazards analysis was used to establish the final prognostic model for HCC patients. *MYOCD*, Myocardin; *QRFPR*, Pyroglutamylated RFamide Peptide Receptor; *MMP16*, Matrix Metallopeptidase 16; *CLEC1B*, C-Type Lectin Domain Family 1 Member B; *LCN6*, Lipocalin 6; *MMP7*, Matrix Metallopeptidase 7; *TRBV10-3*, T Cell Receptor Beta Variable 10-3; *AC080038.4*, Uncharacterized Long Non-Coding RNA AC080038.4; *PRDM9*, PR/SET Domain 9; *AC022905.1*, Uncharacterized Long Non-Coding RNA AC022905.1; *SHISA9*, Shisa Family Member 9; *APCDD1L-DT*, APCDD1L Divergent Transcript (Long Non-Coding RNA); *CDX2*, Caudal Type Homeobox 2; *PSMC1P10*, Proteasome 26S Subunit, ATPase 1 Pseudogene 10; *VSTM1*, V-Set and Transmembrane Domain Containing 1.

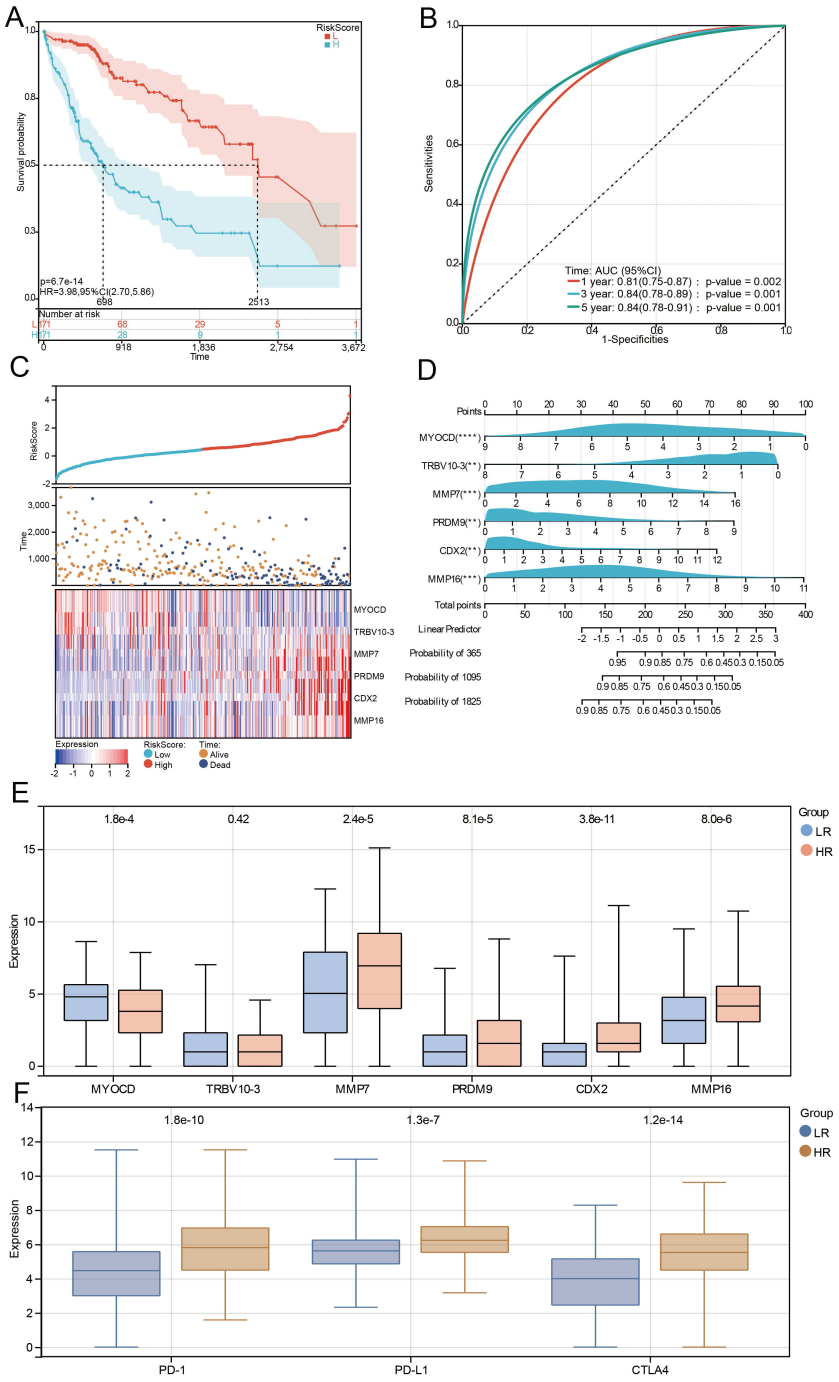

Fig. 3. Validation and performance assessment of the prognostic risk model. (A) Kaplan-Meier survival curves comparing overall survival between high-risk (HR) and low-risk (LR) groups. (B) Time-dependent receiver operating characteristic (ROC) curves evaluating the predictive accuracy of the model at 1-, 3-, and 5-year survival intervals. (C) Prognostic heatmap displaying risk scores, survival outcomes, and expression profiles of the six prognostic genes across patients. (D) Prognostic nomogram developed using the six key prognostic genes from the risk prediction model, constructed with the rms package in R to estimate survival probabilities. The asterisks represent the level of statistical significance of each gene in the multivariate Cox regression model used to develop the nomogram: $**p < 0.01$, $***p < 0.001$, $****p < 0.0001$. (E) Box plots showing expression differences of the six prognostic genes between high- and low-risk groups. (F) Expression analysis of immune checkpoint-related genes between high- and low-risk groups highlighting immune modulation patterns. HR, Hazard Ratio; AUC, area under the ROC curve; CI, confidence interval; *MYOCD*, Myocardin; *TRBV10-3*, T Cell Receptor Beta Variable 10-3; *MMP7*, Matrix Metallopeptidase 7; *PRDM9*, PR/SET Domain 9; *CDX2*, Caudal Type Homeobox 2; *MMP16*, Matrix Metallopeptidase 16; *PD-1*, Programmed Cell Death Protein 1; *PD-L1*, Programmed Death-Ligand 1; *CTLA4*, Cytotoxic T-Lymphocyte–Associated Protein 4; LR, low risk; HR, high risk.

Table 1. Comparison of baseline characteristics between high-risk and low-risk groups.

Variables	Total (n = 342)	High-risk (n = 171)	Low-risk (n = 171)	Statistic	*p*-value
Age, mean ± SD	60.11 ± 13.41	59.73 ± 13.67	60.49 ± 13.17	$t = -0.53$	0.598
Gender, n (%)				$\chi^2 = 0.05$	0.817
Female	110 (32.16)	56 (32.75)	54 (31.58)		
Male	232 (67.84)	115 (67.25)	117 (68.42)		
Tumor stage (T), n (%)				$\chi^2 = 0.90$	0.826
T1	173 (50.58)	89 (52.05)	84 (49.12)		
T2	83 (24.27)	39 (22.81)	44 (25.73)		
T3	76 (22.22)	37 (21.64)	39 (22.81)		
T4	10 (2.92)	6 (3.51)	4 (2.34)		
Lymph node status (N), n (%)				-	0.202
N0	250 (73.10)	131 (76.61)	119 (69.59)		
N1	4 (1.17)	3 (1.75)	1 (0.58)		
NX	88 (25.73)	37 (21.64)	51 (29.82)		
Metastasis (M), n (%)				-	0.224
M0	262 (76.61)	136 (79.53)	126 (73.68)		
M1	4 (1.17)	3 (1.75)	1 (0.58)		
MX	76 (22.22)	32 (18.71)	44 (25.73)		
Clinical stage, n (%)				-	0.587
Stage I	171 (50.00)	87 (50.88)	84 (49.12)		
Stage II	81 (23.68)	38 (22.22)	43 (25.15)		
Stage III	85 (24.85)	42 (24.56)	43 (25.15)		
Stage IV	5 (1.46)	4 (2.34)	1 (0.58)		
Tumor grade, n (%)				$\chi^2 = 2.60$	0.458
G1	45 (13.16)	23 (13.45)	22 (12.87)		
G2	169 (49.42)	91 (53.22)	78 (45.61)		
G3	116 (33.92)	52 (30.41)	64 (37.43)		
G4	12 (3.51)	5 (2.92)	7 (4.09)		

Notes: *t*, *t*-test; χ^2, Chi-square test; -, Fisher-Irwin test; SD, standard deviation.

icant survival difference between the two risk groups, with elevated risk scores strongly associated with poorer OS ($p = 6.7 \times 10^{-14}$) (Fig. 3A). Additionally, time-dependent ROC curve analysis was conducted to evaluate predictive accuracy at 1, 3, and 5 years, yielding AUC values exceeding 0.7 at all-time points, thus confirming good discriminative performance (Fig. 3B).

To determine whether the predictive capacity of the model was influenced by baseline clinical characteristics between the high-risk and low-risk groups, we compared the basic demographics and clinical data of both groups (e.g., age, gender, TNM stage). No statistically significant differences were observed ($p > 0.05$) (Table 1), identifying that risk stratification based on risk score as independent of these variables.

A prognostic heatmap was constructed to visualize the interrelationship between risk scores, survival outcomes, and gene expression profiles. The heatmap revealed an inverse correlation, where higher risk scores were associated with significantly reduced patient survival (Fig. 3C). Furthermore, a nomogram was developed employing the rms package in R, incorporating the six key prognostic genes from the risk score model. This nomogram provides a user-friendly tool for predicting HCC patient survival and offers clinicians a personalized prognostic tool. The C-index of the nomogram was 0.88 (95% CI: 0.79–0.98, *p*-value = 8.26×10^{-16}), indicating excellent predictive performance (Fig. 3D).

Analysis of individual gene expression levels showed that *MYOCD* expression was significantly higher in the low-risk group compared to the high-risk group, demonstrating a protective role ($p < 0.001$). In contrast, *TRBV10-3* expression showed no significant difference between the high- and low-risk groups ($p > 0.05$). The expression levels of *MMP7*, *PRDM9*, *CDX2*, and *MMP16* were significantly elevated in the high-risk group, suggesting their association with enhanced risk ($p < 0.001$) (Fig. 3E). Given that immune checkpoint upregulation may promote tumor immune escape, we further analyzed the expression of immune checkpoint genes in the high- and low-risk cohorts. Significantly higher expression levels of Programmed Cell Death Protein 1 (*PD-1*), *PD-L1*, and Cytotoxic T-Lymphocyte–Associated Protein 4 (*CTLA4*) were observed in the high-risk group ($p < 0.001$), suggesting an increased likelihood of immune evasion in this subgroup (Fig. 3F).

Basic Clinical Information of Samples

This study included surgical liver cancer tissue samples from 20 HCC patients and 24 normal liver tissue sam-

Table 2. Basic clinical characteristics of normal and tumor samples.

Variables	Normal (n = 24)	Tumor (n = 20)	Statistic	*p*-value
Age, mean ± SD	50.58 ± 13.58	50.65 ± 12.36	$t = -0.02$	0.987
Gender, n (%)			$\chi^2 = 1.00$	0.317
Female	12 (50.00)	7 (35.00)		
Male	12 (50.00)	13 (65.00)		
BMI, mean ± SD	24.40 ± 2.47	25.29 ± 2.93	$t = -1.09$	0.280
Tumor stage, n (%)			-	-
T1	-	1 (5.00)		
T2	-	6 (30.00)		
T3	-	9 (45.00)		
T4	-	4 (20.00)		
Post-treatment, n (%)			-	-
Chemotherapy	-	15 (75.00)		
Radiotherapy	-	5 (25.00)		
Alcohol history, n (%)			$\chi^2 = 7.37$	0.007
No	21 (87.50)	10 (50.00)		
Yes	3 (12.50)	10 (50.00)		
Smoking history, n (%)			$\chi^2 = 2.94$	0.087
No	19 (79.17)	11 (55.00)		
Yes	5 (20.83)	9 (45.00)		
Hepatitis history, n (%)			$\chi^2 = 15.21$	<0.001
No	21 (87.50)	6 (30.00)		
Yes	3 (12.50)	14 (70.00)		
Diabetes, n (%)			-	0.027
No	24 (100.00)	15 (75.00)		
Yes	0 (0.00)	5 (25.00)		
Hypertension, n (%)			$\chi^2 = 1.99$	0.158
No	21 (87.50)	13 (65.00)		
Yes	3 (12.50)	7 (35.00)		

ples collected during surgeries performed over the same period. All patients underwent liver cancer resection in the hospital's surgical department. An overview of the patients' clinicopathological characteristics is provided in Table 2. The HCC group consisted of 65% male and 35% female patients. The mean age of the patients was 50.65 ± 12.36 years, and the mean BMI was 25.29 ± 2.93, with no significant differences from the normal range ($p > 0.05$). Based on tumor staging, the liver cancer group included 1 patient with T1, 6 with T2, 9 with T3, and 4 with T4 tumors. All patients received postoperative adjuvant therapy, including chemotherapy and radiotherapy.

The liver cancer group had a significantly higher proportion of individuals with a history of alcohol consumption (50.00% vs. 12.50%, $p = 0.007$) and hepatitis (70.00% vs. 12.50%, $p < 0.001$). A smoking history was more common in the liver cancer group (45.00% vs. 20.83%, $p = 0.087$), although the difference was not statistically significant. The prevalence of diabetes was also higher among the HCC patients (25.00% vs. 0.00%, $p = 0.027$), while the difference in hypertension prevalence between groups was not statistically significant (35.00% vs. 12.50%, $p = 0.158$).

Validation of Immune Evasion Gene Expression in HCC Clinical Samples

To evaluate immune escape-related gene expression, immunohistochemistry (IHC) was employed to compare HCC tissues with normal liver tissues. The analysis revealed that MYOCD was significantly downregulated in HCC tissues, whereas its expression was markedly elevated in normal liver tissues ($p < 0.001$). In contrast, MMP7, MMP16, PRDM9, and CDX2 were significantly upregulated in HCC tissues, suggesting a strong association between these genes, immune evasion, and tumor progression ($p < 0.001$) (Fig. 4A,B). Further analysis of gene expression based on tumor stage showed that MYOCD expression was significantly lower in patients with T3 and T4 tumors compared to those with T1 and T2 ($p < 0.01$), suggesting a possible tumor-suppressive role for MYOCD in HCC development. Conversely, patients at T3 and T4 stages exhibited significantly elevated levels of MMP7, MMP16, PRDM9, and CDX2 compared to those in T1 and T2 ($p < 0.01$) (Fig. 4C), indicating that these genes may lead to tumor progression and enhanced immune evasion in advanced-stage HCC.

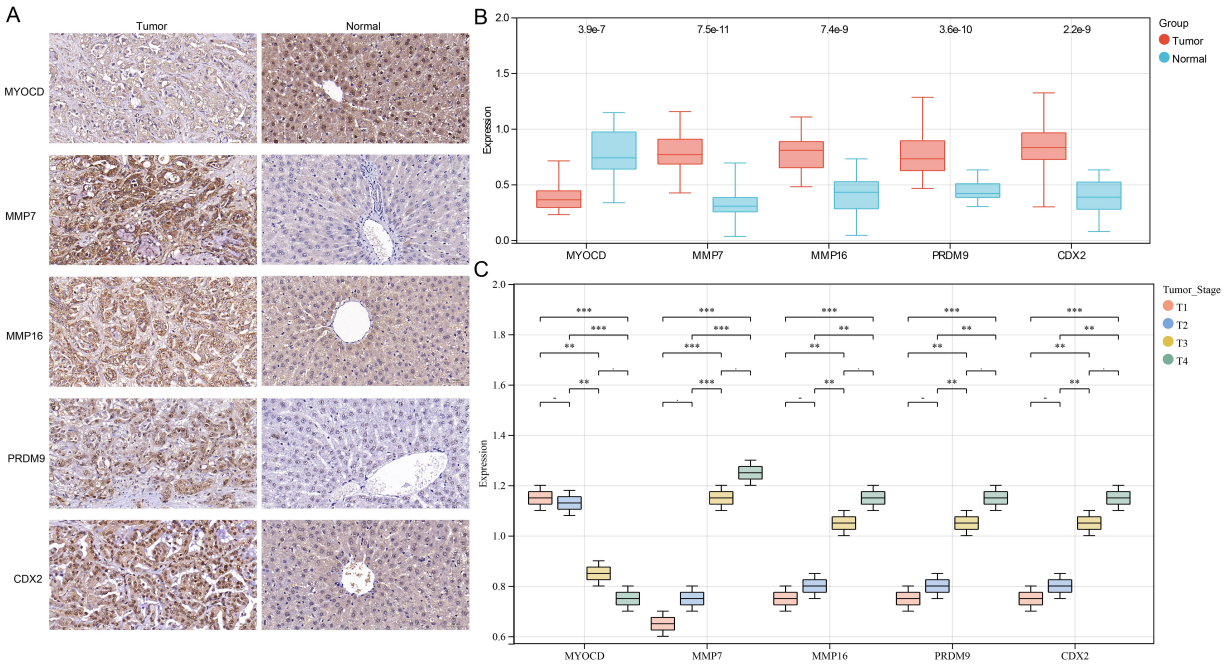

Fig. 4. Expression levels of key genes in HCC and normal tissues. (A,B) Immunohistochemical (IHC) analysis of immune escape-related gene expression in HCC tissue samples (400×). (C) Differential expression of key genes across different tumor stages. $^{**}p < 0.01$, $^{***}p < 0.001$; "-" denotes no statistically significant difference ($p > 0.05$).

Relationship Between Immune Cell Infiltration and Clinical Prognosis

Spearman correlation analysis was conducted using the TIMER database to assess the relationship between infiltration levels of various immune cell subpopulations (including CD8+ T cells, regulatory T cells (Tregs), macrophages, and B cells) and the expression levels of identified key genes (e.g., *MYOCD*, *MMP7*, *MMP16*, *PRDM9*, *CDX2*). In the TCGA-HCC dataset, *MYOCD* expression exhibited a significant negative correlation with B lymphocyte infiltration (r = –0.004) while showing significant positive correlations with CD8+ T lymphocyte (r = 0.142), CD4+ T lymphocyte (r = 0.296), macrophages (r = 0.232), neutrophils (r = 0.275), and dendritic lymphocyte (r = 0.15) ($p < 0.05$) (Fig. 5A, Ref. [19]). *MMP7*, *MMP16*, *PRDM9*, and *CDX2* were all significantly positively correlated with infiltration of B lymphocytes, CD8+ T cells, CD4+ T cells, macrophages, neutrophils, and dendritic cells ($p < 0.05$). Notably, *MMP7* demonstrated a stronger correlation with CD4+ T cells and macrophages (r = 0.347, r = 0.421, respectively), while *MMP16* exhibited a stronger correlation with macrophages, CD4+ T cells, neutrophils, and dendritic cells (r = 0.488, r = 0.432, r = 0.428, r = 0.413, respectively) (Fig. 5B–E).

Further analysis within the TCGA-HCC cohort assessed Stromal, Immune, and ESTIMATE scores for each liver cancer patient, calculated based on the expression profiles of the key genes. The findings revealed that *MYOCD* expression was significantly negatively correlated with both Stromal and ESTIMATE scores ($p < 0.001$) but did not show a significant correlation with the immune score ($p > 0.05$). In contrast, *MMP7* and *MMP16* exhibited significant positive correlations with Stromal, Immune, and ESTIMATE scores ($p < 0.001$). Additionally, *PRDM9* and *CDX2* were significantly positively correlated with the Stromal score ($p < 0.001$ and $p < 0.05$, respectively). However, no significant correlations were observed with either the Immune or ESTIMATE scores ($p > 0.05$) (Fig. 6).

Kaplan-Meier survival analysis was conducted to assess the association between immune cell infiltration and clinical prognosis. The analysis demonstrated that high expression of *MMP7* ($p < 0.01$), *MMP16* ($p < 0.01$), and *CDX2* ($p < 0.05$), as well as downregulation of *MYOCD* ($p < 0.01$), were associated with poorer OS. Conversely, *PRDM9* expression did not show a statistically significant association with patient prognosis ($p > 0.05$) (Fig. 7), suggesting that immune evasion mechanisms may exert differential impacts on clinical outcomes in HCC.

Discussion

Immune evasion is one of the crucial mechanisms underlying tumor development, particularly in malignant cancers such as HCC. Tumor cells employ multiple strategies to evade recognition and elimination by the host's immune system, thereby promoting tumor progression and metastasis [20]. Immune escape-related genes play a crucial role in this process by mediating immune cell infiltration, immune checkpoint expression, intercellular signaling, and

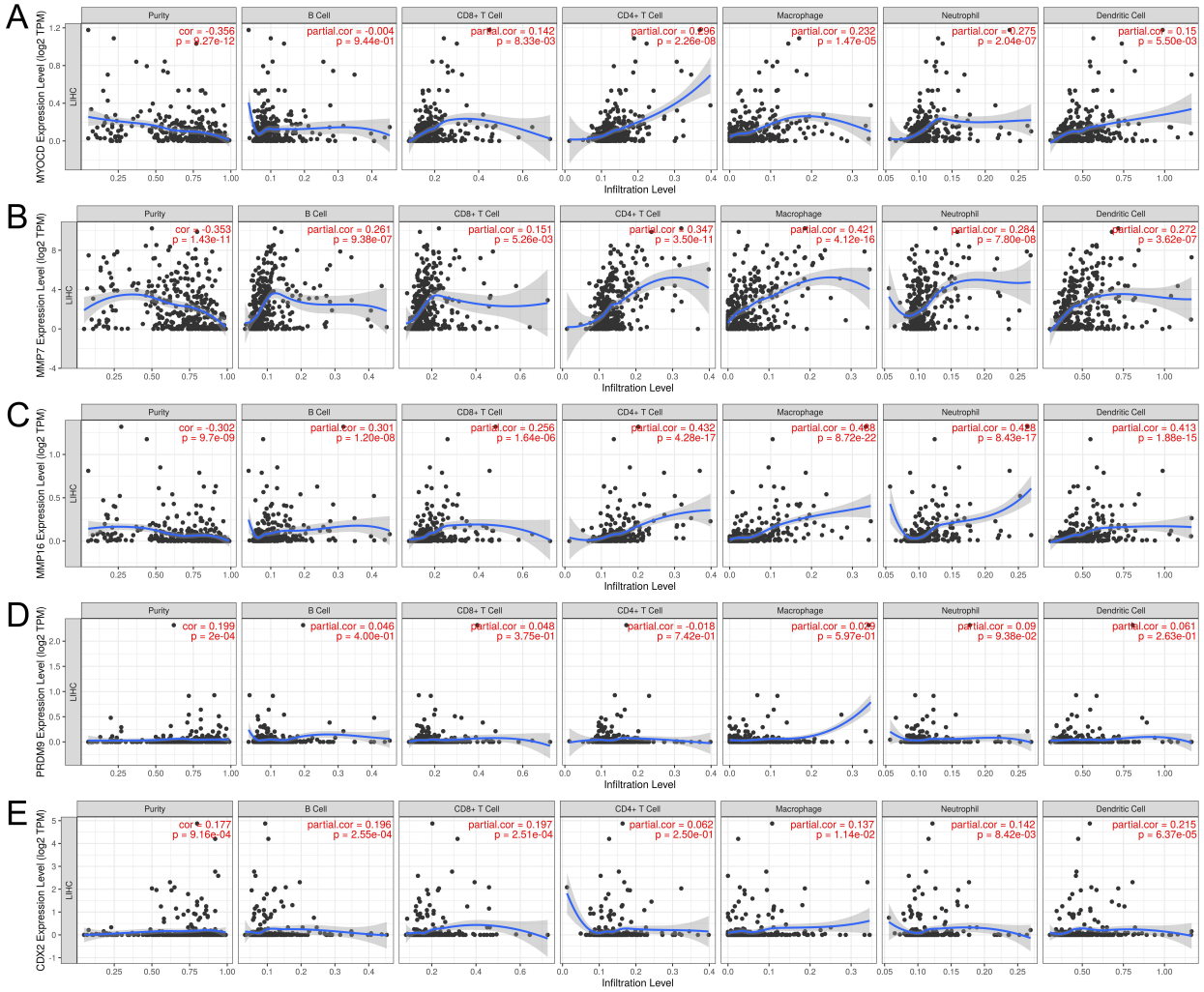

Fig. 5. Correlation between key genes and immune cell infiltration in TCGA-HCC cohort. Correlation of *MYOCD* (A), *MMP7* (B), *MMP16* (C), *PRDM9* (D), and *CDX2* (E) expression with immune cell infiltration levels. The first scatter plot in each panel represents the correlation between gene expression and tumor purity. Genes predominantly expressed in the tumor microenvironment exhibit a negative correlation with tumor purity, while genes highly expressed in tumor cells show a positive correlation [19].

other regulatory mechanisms, allowing liver cancer cells to suppress effective immune responses and facilitate immune evasion [21]. Recent research efforts have increasingly focused on elucidating the molecular mechanisms underlying immune evasion and its impact on tumor progression, therapeutic resistance, and clinical outcomes [22,23]. However, there is still limited knowledge of the specific genes involved in immune escape in HCC, particularly regarding their relationship with immune cell infiltration, immune checkpoints, and associated signaling pathways.

In the present study, immune and stromal scores derived from the TCGA database were utilized to identify DEGs. Functional enrichment, immune cell infiltration analysis, and prognostic modeling were then employed to explore the potential roles of immune escape-related genes in the initiation and progression of HCC. These findings were further validated using surgical HCC and adjacent normal liver tissue samples.

Through the application of immune and stromal scoring, a total of 999 DEGs were identified. GO and KEGG pathway enrichment assessment revealed the biological significance of these DEGs. Notably, their enrichment in immune-related processes such as immune response, adaptive immunity, and complement activation suggested their potential utility as biomarkers for HCC. These DEGs also exhibited significant enrichment in key signaling pathways, including cytokine-receptor interactions, chemokine signaling, Wnt signaling, and Hippo signaling. These pathways have been associated with crucial roles in promoting immune evasion and therapeutic resistance in HCC. Specifically, the Wnt and Hippo signaling pathways are known to play roles in regulating cell proliferation, migration, and immune modulation in HCC. These pathways may contribute to immune evasion by modulating the behavior of immune cells within the TME. The Wnt signaling pathway, in particular, is vital for the initiation, progression, and

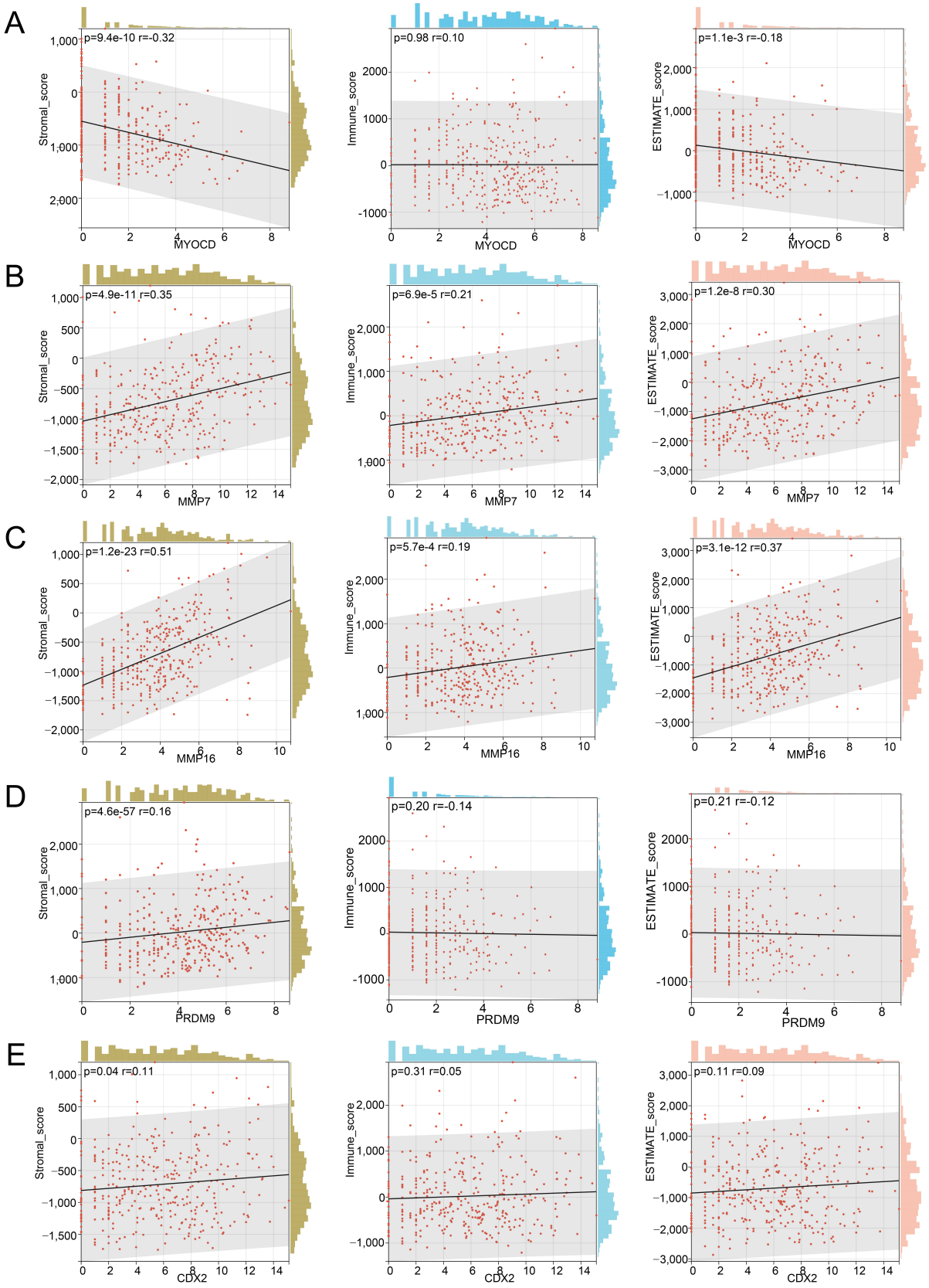

Fig. 6. Correlation of key genes with Stromal score, Immune score, and ESTIMATE score in TCGA-HCC. (A–E) Correlation analysis between gene expression and Stromal score (yellow-green), Immune score (blue), and ESTIMATE (pink) for *MYOCD* (A), *MMP7* (B), *MMP16* (C), *PRDM9* (D), and *CDX2* (E).

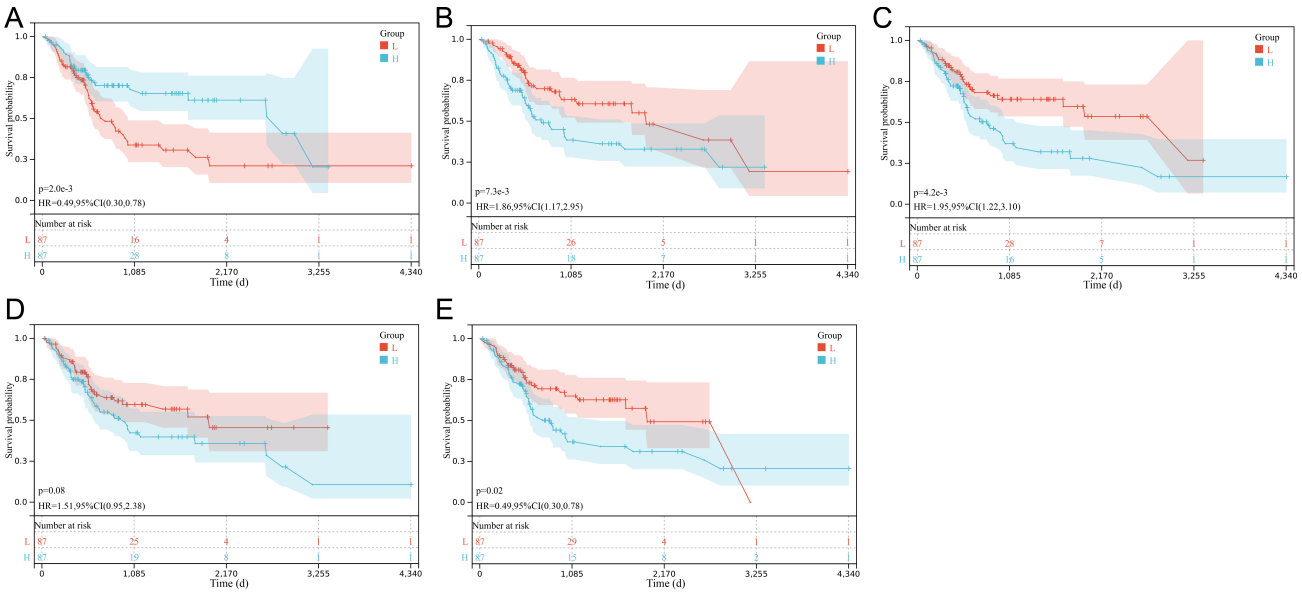

Fig. 7. Prognostic significance of immune cell infiltration assessed via Kaplan-Meier survival analysis. (A–E) Survival curves evaluating the prognostic significance of immune cell infiltration associated with expression levels of *MYOCD* (A), *MMP7* (B), *MMP16* (C), *PRDM9* (D), and *CDX2* (E) in HCC patients.

metastasis of HCC, and may promote immune evasion by modulating the infiltration and function of immune cells. By interacting with various immune cell populations, Wnt signaling may suppress effector T cell activity and enhance the function of immunosuppressive cells [24]. Similarly, the Hippo signaling pathway has been implicated in tumorigenesis and is believed to contribute to immune evasion in HCC through the regulation of cellular proliferation and immune interactions. This pathway may influence immune cell infiltration within the TME, therefore supporting immune evasion mechanisms [25].

A prognostic risk scoring model was developed using LASSO-Cox, univariate and multivariate Cox regression analyses, incorporating six core genes (*MYOCD*, *TRBV10-3*, *MMP7*, *PRDM9*, *CDX2*, and *MMP16*), and its prognostic value was validated using multiple approaches. Kaplan-Meier survival curves revealed statistically significant differences in survival outcomes between high-risk and low-risk groups. The model exhibited excellent predictive performance in ROC curve analyses at 1-, 3-, and 5-year follow-up intervals. Further Cox proportional hazards regression confirmed a significant association between the expression levels of the six core genes and OS in patients with HCC, providing a valuable tool for prognostic assessment in clinical practice.

Immune checkpoint molecules are key mediators of tumor immune evasion. These molecules suppress T-cell activity to facilitate immune escape [26]. The role of the PD-1/PD-L1 signaling pathway in HCC has been well documented. Notably, the ligation of the PD-1 receptor by its ligand *PD-L1* suppresses CD8+ T cell function, consequently weakening antitumor immune responses [27]. *CTLA-4*, another key immune checkpoint, inhibits T cell activation by competitively binding co-stimulatory molecules. Elevated expression of *CTLA-4* in HCC may further impair T cell-mediated antitumor responses, contributing to immune evasion [28]. Our analysis revealed significant upregulation of immune escape-related genes (including *PD-1*, *PD-L1*, and *CTLA4*) in the high-risk cohort, supporting the potential for immune evasion in these patients.

MYOCD (Myocardin) is a transcription factor primarily associated with smooth muscle development and function. It is hypothesized to function as a tumor suppressor gene (TSG), potentially influencing HCC development through epigenetic modulation [29]. A study has demonstrated that downregulation of *MYOCD* can suppress tumor suppressor gene expression in non-small cell lung cancer, suggesting a potential link to immune evasion mechanisms [30]. *TRBV10-3* is a variant gene of the T cell receptor (TCR) β-chain, part of a subfamily of TCR β-chain variable regions (TRBV). Under normal conditions, TCR β-chain rearrangement occurs randomly, but specific TRBV variants may be selectively activated upon antigen stimulation. *TRBV10-3* expression has been shown to significantly change following liver transplantation, indicating its potential role in immune reconstitution and immune escape following transplantation [31]. Based on our findings, we hypothesize that *MYOCD* downregulation may reduce tumor cell sensitivity to the immune system, enhancing immune evasion. By altering the expression of immune regulatory molecules, decreased *MYOCD* levels may impair the immune detection of tumor cells. Likewise, *TRBV10-3* downregulation may result in functional deficits in specific

T cell subsets, thereby weakening immune responses and increasing the tumor's capacity to evade immune surveillance. However, our results showed no statistically significant difference in *TRBV10-3* expression between the high- and low-risk groups. Therefore, our IHC analysis of clinical samples further validated the high expression of *MYOCD*, *MMP7*, *MMP16*, *PRDM9*, and *CDX2* in HCC. *MMP7*, *MMP16*, *PRDM9*, and *CDX2* were upregulated in liver cancer tissues, whereas *MYOCD* was downregulated. These IHC findings were consistent with gene expression data, further supporting the possibility that these genes contribute to immune evasion and tumor progression in HCC.

MMP7 (Matrix Metallopeptidase 7) and *MMP16* are crucial mediators of tumor invasion and metastasis, especially in tumor cell migration and infiltration. Elevated expression of these MMPs likely facilitates tumor invasion and metastasis through the degradation of the extracellular matrix. This process is intricately linked to the pattern of immune cell infiltration and may subsequently promote immune evasion [32,33]. Consistent with the findings of Gao *et al*. [34], our analysis revealed a strong association between high *MMP7* and *MMP16* expression and poor prognosis in HCC patients. Previous studies have indicated that MMPs may contribute to immune escape mechanisms by enhancing tumor invasiveness and metastasis, in part through immunosuppressive effects mediated by the *TGF-β* signaling pathway [35,36] and the splicing of *PD-L1* [37]. Notably, sphingosine-1-phosphate (S1P) has been shown to upregulate *MMP-7* activity in HCC and induce shedding of SDC1 (cell surface proteoglycan), leading to excessive *TGF-β1* production. *TGF-β1* maintains epithelial-mesenchymal transition (EMT) through the *MMP-7/SDC1/aTGF-β1* autocrine loop, thereby enhancing tumor invasiveness [38]. Our data suggest that *MMP7* expression is significantly associated with higher risk scores, indicating a potential role in immune escape mechanisms in HCC.

The PRDM (PRDI-BF1 and RIZ homologous domain) family of transcription factors is known for its regulatory roles in various pathological conditions, including cancers. PRDM1 (also known as BLIMP1) has been shown to promote immune evasion in HCC by modulating *PD-L1* expression, which contributes to T cell exhaustion and subsequent immune escape [39]. Overexpression of *PRDM9* may similarly enhance tumor cell immune tolerance of tumor cells by modulating immune checkpoint molecules and immune regulatory pathways. *CDX2* is a transcription factor primarily involved in the differentiation of gastrointestinal epithelial cells. Abnormal expression of *CDX2* has been linked to cancer progression, including in HCC. Its association with limited survival in HCC suggests a significant role in immune evasion mechanisms [40]. Immune cell infiltration analysis revealed a close relationship between specific immune cell subpopulations and patient survival. Spearman correlation analysis demonstrated that expression levels of immune escape-related genes were associated with decreased infiltration of CD8+ T cells and increased infiltration of macrophages and regulatory T cells (Tregs). This suggests that these genes promote immune tolerance and escape in HCC by modulating the infiltration and function of immune cells, particularly the changes in T cells, macrophages, and dendritic cells.

Our results showed that *MMP7* and *MMP16* were significantly positively correlated with immune cell populations, especially CD4+ T cells, macrophages, and neutrophils. *MMP16* promoted infiltration of immunosuppressive cell types, including Tregs and M2 macrophages, potentially contributing to poor prognosis [41]. A study has indicated that *MMP7* promotes macrophage infiltration and, depending on cancer type, may favor either M1 or M2 macrophage polarization, influencing the balance between pro-inflammatory responses and immune escape [42]. Changes in immune cell infiltration levels were closely associated with clinical outcomes of patients, further underscoring the critical role of immune escape in liver cancer progression.

Based on the discussed analysis, we further developed a nomogram based on the risk score model and validated its predictive performance, achieving a C-index of 0.88. This nomogram provides clinicians with a personalized prognostic assessment tool capable of predicting survival outcomes based on a patient's risk score and aiding in clinical decision-making. Although this study yielded meaningful results through multi-dimensional and multi-level analyses, certain limitations remain. First, the samples from the TCGA database are derived from a public dataset that does not represent populations from all geographic regions and ethnic groups, potentially limiting the generalizability of the findings. Second, the immune cell infiltration analysis using the TIMER database has inherent limitations and may not capture the full diversity of immune cell subpopulations, particularly rare immune cell types or those with altered functional states. Additionally, although the prognostic model was constructed based on existing data, it requires validation in external datasets such as ICGC or GEO, as well as in independent clinical cohorts. Comprehensive functional analyses are also necessary to assess its predictive accuracy and clinical applicability.

In this study, we identified several genes associated with immune escape. However, strategies to effectively overcome these immune evasion mechanisms remain a major challenge. For example, ICIs, such as PD-1 and CTLA-4, can partially restore T cell function, but immune escape mechanisms in HCC are complex and may not be solely mediated by immune checkpoint expression.

Future research should focus on several key areas. First, validation of immune escape mechanisms should be conducted using more diverse and representative sample sources, particularly across different ethnic groups and clinical stages. Second, immune cell infiltration analysis

should be refined by characterizing additional immune cell subpopulations to improve the accuracy of immune status assessments within the TME. Advanced techniques such as single-cell RNA sequencing and flow cytometry should be employed to comprehensively evaluate alterations in immune cell subpopulations, providing deeper insights into immune escape mechanisms in HCC. Additionally, experimental models, such as gene knockout or overexpression approaches, will be valuable to validate the functional roles of genes such as *MYOCD*, *MMP7*, and *PRDM9* in immune evasion. Finally, future studies may explore combination immunotherapeutic strategies, such as concurrent use of ICIs with targeted therapies, cytokine-based therapies, or gene-editing techniques, to enhance therapeutic efficacy.

Conclusion

In conclusion, this research offers novel insights into the molecular mechanisms underlying immune evasion in liver cancer, identifying core genes related to immune escape and successfully constructing a risk-scoring model with strong prognostic predictive performance. These findings present promising biomarkers and potential clinical applications for personalized treatment and prognosis assessment in liver cancer. However, further validation using larger clinical cohorts and animal models is required to confirm the distinct roles of these genes in immune evasion and assess their clinical utility in liver cancer management.

Availability of Data and Materials

The data are available from the authors upon reasonable request.

Author Contributions

ZWB was responsible for data acquisition, analysis, and interpretation, and contributed to the drafting and critical revision of the manuscript. DXF contributed to data analysis and interpretation, and participated in manuscript revision for important intellectual content. XXW jointly participated in data collection and provided critical revision during manuscript preparation. XZL contributed to the interpretation of results and participated in the review and critical revision of the manuscript. ZHZ was responsible for study design, supervision of the research process, and critical revision of the manuscript for intellectual content. All authors have read and approved the final manuscript and agreed to be accountable for all aspects of the work, ensuring the accuracy and integrity of any part of the study.

Ethics Approval and Consent to Participate

This study did not involve the collection of new human or animal samples. All tissue microarrays were commercially obtained from Shanghai Outdo Biotech Co., Ltd., and were pathologically confirmed and anonymized prior to purchase. As the study did not involve direct human participation, identifiable data, or personal health information, institutional ethical approval and informed consent were not required. The study was conducted in accordance with the principles of the Declaration of Helsinki.

Acknowledgement

Not applicable.

Funding

This research received no external funding.

Conflict of Interest

The authors declare no conflict of interest.

References

[1] Sung H, Ferlay J, Siegel RL, Laversanne M, Soerjomataram I, Jemal A, *et al*. Global Cancer Statistics 2020: GLOBOCAN Estimates of Incidence and Mortality Worldwide for 36 Cancers in 185 Countries. CA: A Cancer Journal for Clinicians. 2021; 71: 209–249. https://doi.org/10.3322/caac.21660.

[2] Wang J, Ha J, Lopez A, Bhuket T, Liu B, Wong RJ. Medicaid and Uninsured Hepatocellular Carcinoma Patients Have More Advanced Tumor Stage and Are Less Likely to Receive Treatment. Journal of Clinical Gastroenterology. 2018; 52: 437–443. https://doi.org/10.1097/MCG.0000000000000859.

[3] Alawyia B, Constantinou C. Hepatocellular Carcinoma: a Narrative Review on Current Knowledge and Future Prospects. Current Treatment Options in Oncology. 2023; 24: 711–724. https://doi.org/10.1007/s11864-023-01098-9.

[4] Criss CR, Makary MS. Recent Advances in Image-Guided Locoregional Therapies for Primary Liver Tumors. Biology. 2023; 12: 999. https://doi.org/10.3390/biology12070999.

[5] Xu Z, Hu Y, Huang L. Effectiveness and Safety of Radiofrequency Ablation versus Liver Resection in the Treatment of Early-stage Hepatocellular Carcinoma: A Systematic Review and Meta-analysis. Annali Italiani di Chirurgia. 2024; 95: 109–118. https://doi.org/10.62713/aic.3155.

[6] Shi F, Shi M, Zeng Z, Qi RZ, Liu ZW, Zhang JY, *et al*. PD-1 and PD-L1 upregulation promotes CD8(+) T-cell apoptosis and postoperative recurrence in hepatocellular carcinoma patients. International Journal of Cancer. 2011; 128: 887–896. https://doi.org/10.1002/ijc.25397.

[7] Zeng Z, Yao W, Xu X, Xu G, Long J, Wang X, *et al*. Hepatocellular carcinoma cells deteriorate the biophysical properties of dendritic cells. Cell Biochemistry and Biophysics. 2009; 55: 33–43. https://doi.org/10.1007/s12013-009-9055-6.

[8] Muller M, Schouten RD, De Gooijer CJ, Baas P. Pembrolizumab for the treatment of non-small cell lung cancer. Expert Review of Anticancer Therapy. 2017; 17: 399–409. https://doi.org/10.1080/14737140.2017.1311791.

[9] Wolchok JD, Kluger H, Callahan MK, Postow MA, Rizvi NA, Lesokhin AM, *et al*. Nivolumab plus ipilimumab in advanced melanoma. The New England Journal of Medicine. 2013; 369: 122–133. https://doi.org/10.1056/NEJMoa1302369.

[10] Motzer RJ, Escudier B, McDermott DF, George S, Hammers HJ, Srinivas S, *et al*. Nivolumab versus Everolimus in Advanced Renal-Cell Carcinoma. The New England Journal of

Medicine. 2015; 373: 1803–1813. https://doi.org/10.1056/NEJMoa1510665.

[11] El-Khoueiry AB, Sangro B, Yau T, Crocenzi TS, Kudo M, Hsu C, *et al*. Nivolumab in patients with advanced hepatocellular carcinoma (CheckMate 040): an open-label, non-comparative, phase 1/2 dose escalation and expansion trial. Lancet. 2017; 389: 2492–2502. https://doi.org/10.1016/S0140-6736(17)31046-2.

[12] Cheng AL, Qin S, Ikeda M, Galle PR, Ducreux M, Kim TY, *et al*. Updated efficacy and safety data from IMbrave150: Atezolizumab plus bevacizumab vs. sorafenib for unresectable hepatocellular carcinoma. Journal of Hepatology. 2022; 76: 862–873. https://doi.org/10.1016/j.jhep.2021.11.030.

[13] Cheng K, Cai N, Zhu J, Yang X, Liang H, Zhang W. Tumor-associated macrophages in liver cancer: From mechanisms to therapy. Cancer Communications. 2022; 42: 1112–1140. https://doi.org/10.1002/cac2.12345.

[14] Dong ZZ, Yao DF, Yao M, Qiu LW, Zong L, Wu W, *et al*. Clinical impact of plasma TGF-beta1 and circulating TGF-beta1 mRNA in diagnosis of hepatocellular carcinoma. Hepatobiliary & Pancreatic Diseases International. 2008; 7: 288–295.

[15] Enarsson K, Johnsson E, Lindholm C, Lundgren A, Pan-Hammarström Q, Strömberg E, *et al*. Differential mechanisms for T lymphocyte recruitment in normal and neoplastic human gastric mucosa. Clinical Immunology. 2006; 118: 24–34. https://doi.org/10.1016/j.clim.2005.08.001.

[16] Jiang HY, Chen J, Xia CC, Cao LK, Duan T, Song B. Noninvasive imaging of hepatocellular carcinoma: From diagnosis to prognosis. World Journal of Gastroenterology. 2018; 24: 2348–2362. https://doi.org/10.3748/wjg.v24.i22.2348.

[17] Du J, Tao Q, Liu Y, Huang Z, Jin H, Lin W, *et al*. Assessment of the targeted effect of Sijunzi decoction on the colorectal cancer microenvironment via the ESTIMATE algorithm. PLoS ONE. 2022; 17: e0264720. https://doi.org/10.1371/journal.pone.0264720.

[18] Jia D, Li S, Li D, Xue H, Yang D, Liu Y. Mining TCGA database for genes of prognostic value in glioblastoma microenvironment. Aging. 2018; 10: 592–605. https://doi.org/10.18632/aging.101415.

[19] Zhang Y, Zhang C, He M, Xing W, Hou R, Zhang H. Co-expression of IL-21-Enhanced NKG2D CAR-NK cell therapy for lung cancer. BMC Cancer. 2024; 24: 119. https://doi.org/10.1186/s12885-023-11806-1.

[20] Du G, Dou C, Sun P, Wang S, Liu J, Ma L. Regulatory T cells and immune escape in HCC: understanding the tumor microenvironment and advancing CAR-T cell therapy. Frontiers in Immunology. 2024; 15: 1431211. https://doi.org/10.3389/fimmu.2024.1431211.

[21] Cheng Q, Wang W, Liu J, Lv Z, Ji W, Yu J, *et al*. Elevated *MPP6* expression correlates with an unfavorable prognosis, angiogenesis and immune evasion in hepatocellular carcinoma. Frontiers in Immunology. 2023; 14: 1173848. https://doi.org/10.3389/fimmu.2023.1173848.

[22] Liu Y, Han YS, Wang JF, Pang ZQ, Wang JS, Zhang L, *et al*. A new immune-related gene signature predicts the prognosis and immune escape of bladder cancer. Cancer Biomarkers: Section a of Disease Markers. 2023; 38: 567–581. https://doi.org/10.3233/CBM-230190.

[23] Tang S, Ning Q, Yang L, Mo Z, Tang S. Mechanisms of immune escape in the cancer immune cycle. International Immunopharmacology. 2020; 86: 106700. https://doi.org/10.1016/j.intimp.2020.106700.

[24] Yuan Y, Wu D, Hou Y, Zhang Y, Tan C, Nie X, *et al*. Wnt signaling: Modulating tumor-associated macrophages and related immunotherapeutic insights. Biochemical Pharmacology. 2024; 223: 116154. https://doi.org/10.1016/j.bcp.2024.116154.

[25] Li L, Wang LL, Wang TL, Zheng FM. ACADL suppresses PD-L1 expression to prevent cancer immune evasion by targeting Hippo/YAP signaling in lung adenocarcinoma. Medical Oncology. 2023; 40: 118. https://doi.org/10.1007/s12032-023-01978-y.

[26] Cai M, Xu M, Yu D, Wang Q, Liu S. Posttranslational regulatory mechanism of PD-L1 in cancers and associated opportunities for novel small-molecule therapeutics. Acta Biochimica et Biophysica Sinica. 2024; 56: 1415–1424. https://doi.org/10.3724/abbs.2024085.

[27] Ju F, Wang D, Huang L, Jiang C, Gao C, Xiong C, *et al*. Progress of PD-1/PD-L1 signaling in immune response to liver transplantation for hepatocellular carcinoma. Frontiers in Immunology. 2023; 14: 1227756. https://doi.org/10.3389/fimmu.2023.1227756.

[28] Xu J, Wu X, Wang X. Ferroptosis-Related Genes with Regard to CTLA-4 and Immune Infiltration in Hepatocellular Carcinoma. Biochemical Genetics. 2023; 61: 687–703. https://doi.org/10.1007/s10528-022-10279-4.

[29] Xie CR, Sun H, Wang FQ, Li Z, Yin YR, Fang QL, *et al*. Integrated analysis of gene expression and DNA methylation changes induced by hepatocyte growth factor in human hepatocytes. Molecular Medicine Reports. 2015; 12: 4250–4258. https://doi.org/10.3892/mmr.2015.3974.

[30] Shafi O, Siddiqui G, Jaffry HA. The benign nature and rare occurrence of cardiac myxoma as a possible consequence of the limited cardiac proliferative/ regenerative potential: a systematic review. BMC Cancer. 2023; 23: 1245. https://doi.org/10.1186/s12885-023-11723-3.

[31] Yang G, Ou M, Chen H, Guo C, Chen J, Lin H, *et al*. Characteristic analysis of TCR β-chain CDR3 repertoire for pre- and post-liver transplantation. Oncotarget. 2018; 9: 34506–34519. https://doi.org/10.18632/oncotarget.26138.

[32] Chen L, Li M, Li Q, Wang CJ, Xie SQ. DKK1 promotes hepatocellular carcinoma cell migration and invasion through β-catenin/MMP7 signaling pathway. Molecular Cancer. 2013; 12: 157. https://doi.org/10.1186/1476-4598-12-157.

[33] Yan P, Wang J, Liu H, Liu X, Fu R, Feng J. M1 macrophage-derived exosomes containing miR-150 inhibit glioma progression by targeting MMP16. Cellular Signalling. 2023; 108: 110731. https://doi.org/10.1016/j.cellsig.2023.110731.

[34] Gao Q, Wang XY, Qiu SJ, Zhou J, Shi YH, Zhang BH, *et al*. Tumor stroma reaction-related gene signature predicts clinical outcome in human hepatocellular carcinoma. Cancer Science. 2011; 102: 1522–1531. https://doi.org/10.1111/j.1349-7006.2011.01981.x.

[35] Krstic J, Santibanez JF. Transforming growth factor-beta and matrix metalloproteinases: functional interactions in tumor stroma-infiltrating myeloid cells. The Scientific World Journal. 2014; 2014: 521754. https://doi.org/10.1155/2014/521754.

[36] Qin G, Luo M, Chen J, Dang Y, Chen G, Li L, *et al*. Reciprocal activation between MMP-8 and TGF-β1 stimulates EMT and malignant progression of hepatocellular carcinoma. Cancer Letters. 2016; 374: 85–95. https://doi.org/10.1016/j.canlet.2016.02.001.

[37] Kiriyama Y, Nochi H. Regulation of PD-L1 Expression by Nuclear Receptors. International Journal of Molecular Sciences. 2023; 24: 9891. https://doi.org/10.3390/ijms24129891.

[38] Zeng Y, Liu X, Yan Z, Xie L. Sphingosine 1-phosphate regulates proliferation, cell cycle and apoptosis of hepatocellular carcinoma cells via syndecan-1. Progress in Biophysics and Molecular Biology. 2019; 148: 32–38. https://doi.org/10.1016/j.pbiomolbio.2017.11.006.

[39] Li Q, Zhang L, You W, Xu J, Dai J, Hua D, *et al*. PRDM1/BLIMP1 induces cancer immune evasion by modulating the USP22-SPI1-PD-L1 axis in hepatocellular carcinoma cells. Nature Communications. 2022; 13: 7677. https://doi.org/

10.1038/s41467-022-35469-x.

[40] Shah SS, Wu TT, Torbenson MS, Chandan VS. Aberrant CDX2 expression in hepatocellular carcinomas: an important diagnostic pitfall. Human Pathology. 2017; 64: 13–18. https://doi.org/10.1016/j.humpath.2016.12.029.

[41] Zhao T, Li X, Li M, Jamil M, Zhang J. Characterization and verification of MMP family members as potential biomarkers in kidney clear cell renal carcinoma. American Journal of Cancer Research. 2023; 13: 3941–3962.

[42] Meng N, Li Y, Jiang P, Bu X, Ding J, Wang Y, *et al*. A Comprehensive Pan-Cancer Analysis of the Tumorigenic Role of Matrix Metallopeptidase 7 (MMP7) Across Human Cancers. Frontiers in Oncology. 2022; 12: 916907. https://doi.org/10.3389/fonc.2022.916907.